Electronic structure and optical absorption of GaAs/$Al_xGa_{1-x}As$ and $Al_xGa_{1-x}As$/GaAs core-shell nanowires

V. V. Ravi Kishore, B. Partoens, and F. M. Peeters
Department of Physics, University of Antwerp, Groenenborgerlaan 171, 2020 Antwerp, Belgium
(Received 10 September 2010; published 14 December 2010)

The electronic structure of GaAs/$Al_xGa_{1-x}As$ and $Al_xGa_{1-x}As$/GaAs core-shell nanowires grown in the [001] direction is studied. The $\mathbf{k}\cdot\mathbf{p}$ method with the 6×6 Kohn-Lüttinger Hamiltonian, taking into account the split-off band is used. The variation in the energy level dispersion, the spinor contribution to the ground state and the optical interband absorption are studied. For some range of parameters the top of the valence band exhibits a camelback structure which results in an extra peak in the optical absorption.

DOI: 10.1103/PhysRevB.82.235425 PACS number(s): 73.21.Hb, 73.22.−f, 78.67.Lt, 78.67.Uh

I. INTRODUCTION

Nanowires posses the unique property of one dimensional quantum confinement and have emerged as promising structures in applications for future electronics and photonics. With the advent of new growth techniques such as the vapor-liquid-solid[1] technique and molecular-beam epitaxy[2] techniques, nanowires can be synthesized with different materials, different shapes and sizes. Using these techniques nanowires of group IV semiconductors [Si (Refs. 3 and 4) and Ge (Ref. 5)] and semiconducting compounds of groups III-V and II-VI [InAs,[6] GaAs,[7,8] and CdSe (Ref. 9)] have been synthesized. Due to the high dielectric mismatch between the nanowire and its surroundings, optical confinement can be achieved and hence nanowires can form important lasing devices.[10] The one-dimensional quantum confinement can be used for future information storage and processing.[11] Typically, these nanowires have either a zinc-blende or diamondlike structure and can be grown in [001], [110], or [111] crystallographic directions which depend on the material, the substrate and also the growth technique used. This has been confirmed by direct imaging of the atomic structure of nanowires.[12]

Free-standing nanowires can be grown as either single material,[13] core-shell, or multishell[14,15] nanowires. The core-shell structures have a core, surrounded by one or more shells of different materials. Core-shell nanowires have been proposed for photovoltaic devices[16] with *p*-doped core and *n*-doped shell acting as a *p*-*n* junction. Also such *p*-*n* junctions formed in core-shell structures can be used to build nanolight-emitting diodes.[17] Building of nanowire lasers with core-shell structures operating in the near-infrared spectral region has been achieved.[18] Nanoscale devices like photodetectors[19] and field effect transistors[20] have gathered a lot of attention in the recent past. In all these devices the knowledge of their electronic structure is essential to understand their device operation.

Electronic properties of core-shell structures have been studied by various authors.[21,22] It has been claimed that for core-shell nanowires composed of lattice-matched materials (e.g., GaAs and AlAs), the electronic structure is trivial.[23] However, in this paper we show that the electronic structure of unstrained core-shell wires can differ significantly from the corresponding single material wires.

In this paper, we consider an infinitely long cylindrical core-shell nanowire as schematically shown in Fig. 1 and study its electronic properties using the multiband $\mathbf{k}\cdot\mathbf{p}$ method. We consider wires grown in the [001] direction consisting of GaAs and $Al_xGa_{1-x}As$, taking one material as the core and the other as the shell material. Here we consider very thin nanowires of diameter $d=2-12$ nm. As in GaAs the Bohr radius is $a_B\simeq11.5$ nm and the effective Rydberg energy $E_{Ry}\simeq5.0$ meV, quantum confinement effects are very important in these thin nanowires.

This paper is organized as follows. In the next section we give the theoretical description of our model. In Sec. III we present our results for the single-particle states, starting with a discussion of GaAs and how spin-orbit interaction modifies the valence band-energy dispersion, spinor distribution, and density. This is followed by results on $Al_xGa_{1-x}As$ free-standing nanowires. And finally we present our results for the core-shell nanowire with GaAs as core and $Al_xGa_{1-x}As$ as shell and vice versa. Our results are summarized in Sec. IV.

II. THEORY

The $\mathbf{k}\cdot\mathbf{p}$ method is applicable for direct-wide gap semiconductors (e.g., GaAs, CdTe, etc.). In the $\mathbf{k}\cdot\mathbf{p}$ method the Hamiltonian is expanded around $k_z=0$. The $\mathbf{k}\cdot\mathbf{p}$ method is used in various models like Kane's model (which includes spin-orbit interaction) and Pikus-Bir Hamiltonian (which includes strain).[24,25]

In this paper for the conduction band we consider a parabolic energy spectrum with effective mass m^*. The dispersion of the conduction band is given by

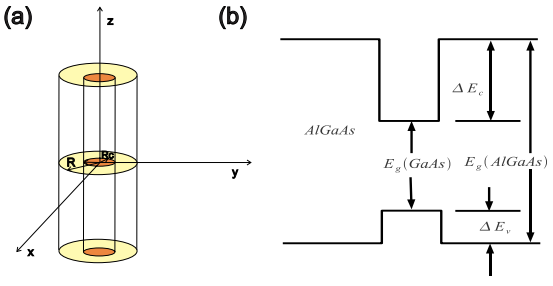

FIG. 1. (Color online) (a) Cylindrical core-shell nanowire and (b) radial band alignment in a GaAs/AlGaAs heterostructure.

$$H_{el} = \frac{\hbar^2}{2m^*}(k_x^2 + k_y^2 + k_z^2). \tag{1}$$

For the valence band we use the 6×6 Kohn-Lüttinger (KL) Hamiltonian for zinc-blende crystal structures[26–28] which includes the spin-orbit interaction. We do not make any further approximations such as the axial or spherical approximation.[29] This KL Hamiltonian is given by

$$H_{\mathrm{KL}} = -\begin{pmatrix} P+Q & -S & R & 0 & -\frac{1}{\sqrt{2}}S & \sqrt{2}R \\ -S^\dagger & P-Q & 0 & R & -\sqrt{2}Q & \sqrt{\frac{3}{2}}S \\ R^\dagger & 0 & P-Q & S & \sqrt{\frac{3}{2}}S^\dagger & \sqrt{2}Q \\ 0 & R^\dagger & S^\dagger & P+Q & -\sqrt{2}R^\dagger & -\frac{1}{\sqrt{2}}S^\dagger \\ -\frac{1}{\sqrt{2}}S^\dagger & -\sqrt{2}Q^\dagger & \sqrt{\frac{3}{2}}S & -\sqrt{2}R & P+\Delta_{SO} & 0 \\ \sqrt{2}R^\dagger & \sqrt{\frac{3}{2}}S^\dagger & \sqrt{2}Q^\dagger & -\frac{1}{\sqrt{2}}S & 0 & P+\Delta_{SO} \end{pmatrix} \tag{2}$$

and its matrix elements for the [001] growth direction are

$$P = \frac{\hbar^2}{2m_0}\gamma_1\{k_x^2 + k_y^2 + k_z^2\}, \tag{3a}$$

$$Q = \frac{\hbar^2}{2m_0}\gamma_2\{k_x^2 + k_y^2 - 2k_z^2\}, \tag{3b}$$

$$R = \frac{\hbar^2}{2m_0}\{\sqrt{3}[-\gamma_2(k_x^2 - k_y^2) + 2i\gamma_3 k_x k_y]\}, \tag{3c}$$

$$S = \frac{\hbar^2}{2m_0}\{2\sqrt{3}[\gamma_3(k_x - ik_y)k_z]\} \tag{3d}$$

with

$$\widehat{k_\alpha} = -i\left(\frac{\partial}{\partial\alpha}\right), \quad \alpha = (x,y,z). \tag{4}$$

For our core-shell heterostructure the effective electron mass and Lüttinger parameters can be written as

$$m^* = m_s^* + (m_c^* - m_s^*)[1 - \Theta(\rho - R_c)], \tag{5}$$

$$\gamma = \gamma_s + (\gamma_c - \gamma_s)[1 - \Theta(\rho - R_c)] \tag{6}$$

with m_s^* and γ_s the values in the shell and m_c^* and γ_c the values in the core. Θ is the heavy side step function. R is the radius of the total wire and R_c the radius of the core part. Applying the effective mass approach leads to the following electron Hamiltonian:

$$H_{el} = \frac{\hbar^2}{2}\left\{\frac{1}{2}\left[\widehat{k_+}\frac{1}{m^*}\widehat{k_-} + \widehat{k_-}\frac{1}{m^*}\widehat{k_+}\right] + \widehat{k_z}\frac{1}{m^*}\widehat{k_z}\right\}. \tag{7}$$

The matrix elements of the KL Hamiltonian for our cylindrical core-shell heterostructure are given by[21,22]

$$P+Q = \frac{\hbar^2}{2m_0}\left\{\frac{1}{2}[\widehat{k_+}(\gamma_1+\gamma_2)\widehat{k_-} + \widehat{k_-}(\gamma_1+\gamma_2)\widehat{k_+}] + \widehat{k_z}(\gamma_1 - 2\gamma_2)\widehat{k_z}\right\}, \tag{8a}$$

$$P-Q = \frac{\hbar^2}{2m_0}\left\{\frac{1}{2}[\widehat{k_+}(\gamma_1-\gamma_2)\widehat{k_-} + \widehat{k_-}(\gamma_1-\gamma_2)\widehat{k_+}] + \widehat{k_z}(\gamma_1 + 2\gamma_2)\widehat{k_z}\right\}, \tag{8b}$$

$$R = \frac{-\hbar^2}{2m_0}\{\sqrt{3}[\widehat{k_-}\bar{\gamma}\widehat{k_-} + \widehat{k_+}\mu\widehat{k_+}]\}, \tag{8c}$$

$$S = \frac{\hbar^2}{2m_0}\{\sqrt{3}[\widehat{k_-}\gamma_3\widehat{k_z} + \widehat{k_z}\gamma_3\widehat{k_-}]\}, \tag{8d}$$

where

$$\widehat{k_\pm} = k_x \pm ik_y = -ie^{\pm i\varphi}\left(\frac{\partial}{\partial\rho} \pm \frac{i}{\rho}\frac{\partial}{\partial\varphi}\right), \tag{9}$$

TABLE I. Band parameters of GaAs, AlAs, and $Al_xGa_{1-x}As$ (m_0 is the bare electron mass).

	GaAs	AlAs	$Al_xGa_{1-x}As$	$Al_{0.3}Ga_{0.7}As$
γ_1	6.98	3.76	$(0.4398+0.217x)/(0.0630+0.88x+0.024x^2)$	5.5096
γ_2	2.06	0.82	$(0.2596+0.0269x)/(0.1260+1.76x+0.048x^2)$	1.4604
γ_3	2.93	1.42	$(0.815+0.0305x)/(0.2784+0.296x+0.0308x^2)$	2.2379
m_{lh}	$0.0901m_0$	$0.1852m_0$	$0.0901m_0+(0.0951m_0)x$	$0.1622m_0$
m_{hh}	$0.3497m_0$	$0.4717m_0$	$0.3497m_0+(0.122m_0)x$	$0.3863m_0$
m_e	$0.067m_0$	$0.12m_0$	$0.067m_0+(0.083m_0)x$	$0.0919m_0$
Δ_{so}	−341 meV	−280 meV	$-341+61x$ meV	−322.7 meV
E_g^Γ	1519 meV	3099 meV	$1519+1707x-1437x^2+1310x^3$ meV	1937.1 meV

$$\widehat{k_\pm}(\gamma_s+(\gamma_c-\gamma_s)[1-\Theta(\rho-R_c)])=i(\gamma_c-\gamma_s)\delta(\rho-R_c)e^{\pm i\varphi}, \tag{10}$$

and $\bar{\gamma}=(\gamma_3+\gamma_2)/2$ and $\mu=(\gamma_2-\gamma_3)/2$.

We assume that in our case the charge is totally localized in the nanowire and it is zero outside. All the band parameters used in this paper are taken from the work of Vurgaftman[30] and are given in Table I.

The core-shell nanowire is a heterostructure and hence inclusion of band offset in the Hamiltonian is essential. We use the following band offset values, corresponding to the sign convention in Fig. 1, for the GaAs and $Al_xGa_{1-x}As$ heterostructure:[31] $\Delta E_v=570x$ meV and $\Delta E_c=870x$ meV. The envelope wave function for the conduction band is expanded in a basis of eigenfunctions of a cylinder with radius R,

$$\Psi_{el}^{\sigma}(\rho,\phi,z,\sigma)=e^{ik_z}\sum_{m=-M}^{M}\sum_{l=1}^{L}\times C_{ml}^{el}\frac{e^{im\phi}}{\sqrt{2\pi}}\frac{\sqrt{2}}{RJ_{m+1}(\alpha_{ml})}J_m\left(\alpha_{ml}\frac{\rho}{R}\right)\eta_\sigma, \tag{11}$$

where J_m is the Bessel function of the first kind and α_{ml} is the lth zero of the corresponding bessel function J_m ($m=0,\pm1,\pm2,\pm3,\ldots,\pm M, l=1,2,3,\ldots,L$) and R is the radius of the nanowire. Here we have used cylindrical coordinates (ρ,ϕ,z). The coefficients C_{ml}^{el} are determined by diagonalizing the electron Hamiltonian. Only for pure single material nanowires, the chosen basis functions are eigenfunctions of the electron Hamiltonian. Eigen energies form a set of subbands numbered by pairs (m,l) and are fourfold degenerate with respect to the spin degree of freedom ($\sigma=\pm$) and the angular momentum ($\pm m$). In Eq. (11), the symbol η_σ is the spin part of the electron wave function. For the valence band, for each spinor component, we assumed the following trial wave function:

$$\Psi_h^{\nu}(\rho,\phi,z,\nu)=e^{ik_z}\sum_{m=-M}^{M}\sum_{l=1}^{L}C_{ml}^{\nu}\frac{e^{im\phi}}{\sqrt{2\pi}}\frac{\sqrt{2}}{RJ_{m+1}(\alpha_{ml})}J_m\left(\alpha_{ml}\frac{\rho}{R}\right), \tag{12}$$

where C_{ml}^{ν} are determined by diagonalizing the 6×6 Kohn-Lüttinger Hamiltonian. We limited the infinite sum to typically $M=4$ and $L=4$.

According to the Fermi golden rule[32] the absorption power of photons with energy $E=\hbar\omega$ is given by

$$P=\frac{\pi e^2}{2\omega}\Sigma_{i,f}(F_i-F_f)|\langle f|\vec{p}\cdot\vec{A}|i\rangle|^2\delta[E_f-(E_i+\hbar\omega)], \tag{13}$$

where $F_{i/f}$ is the Fermi-Dirac distribution function with initial (i) and final (f) electronic states, respectively. The initial state corresponds to the valence-band state $\langle\vec{r}|i\rangle=\Sigma_\mu\Psi_h^{\nu}(\vec{r},\mu)\langle\vec{r}|\mu\rangle$ and the final state corresponds to the conduction-band state $\langle\vec{r}|f\rangle=\Psi_{el}^{\sigma}(\vec{r})\langle\vec{r}|S\rangle$, where $\langle\vec{r}|\mu\rangle$ and $\langle\vec{r}|S\rangle$ are Bloch states at the Γ point of the Brillouin zone. For three different polarizations of light, the integral $I=|\langle f|\vec{p}\cdot\vec{A}|i\rangle|^2$ was calculated as follows:

$$I_{\sigma^+}\simeq\left|\frac{2}{\sqrt{6}}\langle\Psi_{el,\uparrow}^{\sigma}|\Psi_{h,3/2,-1/2}^{\nu}\rangle+\frac{2}{\sqrt{2}}\langle\Psi_{el,\downarrow}^{\sigma}|\Psi_{h,3/2,-3/2}^{\nu}\rangle-\frac{2}{\sqrt{3}}\langle\Psi_{el,\uparrow}^{\sigma}|\Psi_{h,1/2,-1/2}^{\nu}\rangle\right|^2, \tag{14a}$$

$$I_{\sigma^-}\simeq\left|\frac{2}{\sqrt{2}}\langle\Psi_{el,\uparrow}^{\sigma}|\Psi_{h,3/2,3/2}^{\nu}\rangle+\frac{2}{\sqrt{6}}\langle\Psi_{el,\downarrow}^{\sigma}|\Psi_{h,3/2,1/2}^{\nu}\rangle+\frac{2}{\sqrt{3}}\langle\Psi_{el,\downarrow}^{\sigma}|\Psi_{h,1/2,1/2}^{\nu}\rangle\right|^2, \tag{14b}$$

for circular polarized light and

$$I_{\pi}\simeq\left|\sqrt{\frac{2}{3}}\langle\Psi_{el,\downarrow}^{\sigma}|\Psi_{h,3/2,-1/2}^{\nu}\rangle+\sqrt{\frac{2}{3}}\langle\Psi_{el,\uparrow}^{\sigma}|\Psi_{h,3/2,1/2}^{\nu}\rangle+\sqrt{\frac{1}{3}}\langle\Psi_{el,\uparrow}^{\sigma}|\Psi_{h,1/2,-1/2}^{\nu}\rangle+\sqrt{\frac{1}{3}}\langle\Psi_{el,\downarrow}^{\sigma}|\Psi_{h,1/2,1/2}^{\nu}\rangle\right|^2, \tag{15}$$

for linearly polarized light.

We also define the degree of circular polarization as

$$\Pi=\frac{I_{\sigma_+}-I_{\sigma_-}}{I_{\sigma_+}+I_{\sigma_-}}. \tag{16}$$

III. RESULTS

We follow the previous work of Redliński and Peeters,[33] and calculate first the energy dispersion and spinor distribu-

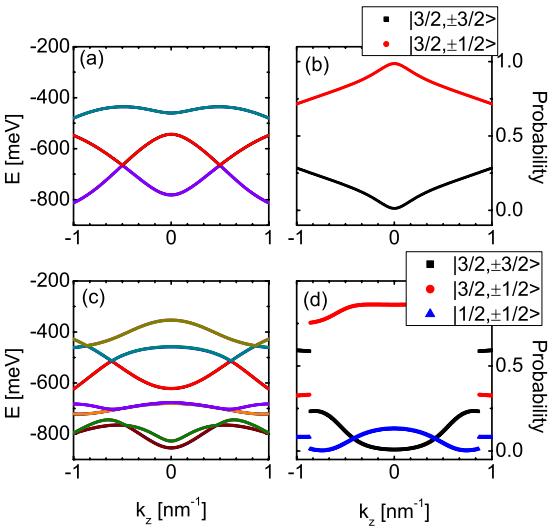

FIG. 2. (Color online) Valence band (left figures) and spinor distribution in the top valence band (right figures) of GaAs nanowire of $R=1.5$ nm with [(a) and (b)] 4×4 KL Hamiltonian and [(c) and (d)] 6×6 KL Hamiltonian.

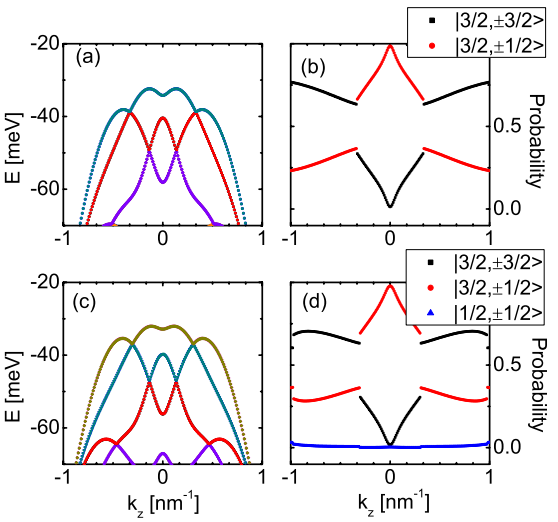

FIG. 3. (Color online) The same as Fig. 2 but now for a nanowire of radius $R=5.5$ nm.

tions for free-standing pure GaAs and $Al_xGa_{1-x}As$ nanowires. In all figures we show also the contributions of the hole states $|\frac{3}{2},\frac{3}{2}\rangle$, $|\frac{3}{2},-\frac{3}{2}\rangle$, $|\frac{3}{2},\frac{1}{2}\rangle$, and $|\frac{3}{2},-\frac{1}{2}\rangle$. In addition the electron and hole densities and the absorption spectra for GaAs, $Al_xGa_{1-x}As$ and their core-shell nanowires are reported. The maximum of the valence band of bulk GaAs is taken as the zero energy in all the energy spectrum plots.

A. Single material nanowire

In Ref. 33 a camelback structure in the energy band structure was found for pure GaAs nanowires and they concluded that this was due to the heavy-hole-light-hole interaction. They reported that this camelback structure decreases with increasing radius of the nanowire.

We extended those results with a special emphasis on the influence of the split-off band and the quantum confinement effects, i.e., we considered an ultrathin pure GaAs nanowire with $R=1.5$ nm. From Fig. 2(a) we find that the 4×4 KL Hamiltonian generates a camelback structure, which is absent in the results obtained from the 6×6 KL Hamiltonian [Fig. 2(c)]. Figures 2(b) and 2(d) show the corresponding spinor distributions. Note that the light-hole contribution has a different behavior as function of k_z: in case of the result obtained with the 4×4 KL Hamiltonian, and where a camelback structure is observed, the contribution is peaked around $k_z=0$, while it is much more flat in the result obtained with the 6×6 KL Hamiltonian, where no camelback structure is found. A look at the different spinor contributions to the hole ground state tells us that the split-off band contribution for a nanowire with very small radius is not negligible. This is not the case for a nanowire of radius $R=5.5$ nm as shown in Fig. 3, where the 4×4 and 6×6 KL Hamiltonians lead to practically the same results with a clear camelback structure. Thus we may conclude that quantum confinement enhances strongly the split-off band contribution and that it can even destroy the camelback structure. From now on all results are obtained with the 6×6 KL Hamiltonian.

Now we investigate the influence of alloying with Al on the camelback structure of the hole band. Figure 4 shows the valence band structure for an $Al_xGa_{1-x}As$ nanowire with radius $R=5.5$ nm for different Al concentrations. Comparison with the result for the pure GaAs nanowire with the same radius [see Fig. 3(d)] learns that the camelback structure slowly vanishes with increasing x.

B. Core-shell nanowires

The camelback structure of the lowest valence band is a remarkable feature of the electronic structure in pure GaAs nanowires and to a lesser extent in pure $Al_xGa_{1-x}As$ nanowires. Now we will investigate how this valence band structure is affected in core-shell nanowires. As shown above, the

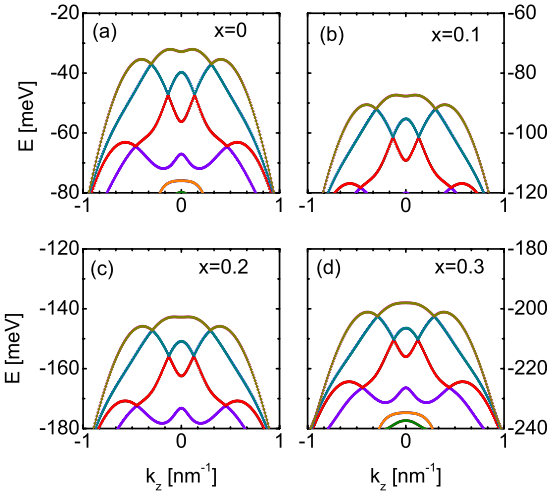

FIG. 4. (Color online) Valence band structure with (a) $x=0$, (b) $x=0.1$, (c) $x=0.2$, and (d) $x=0.3$ with $R=5.5$ nm $Al_xGa_{1-x}As$ nanowire in [001] growth direction.

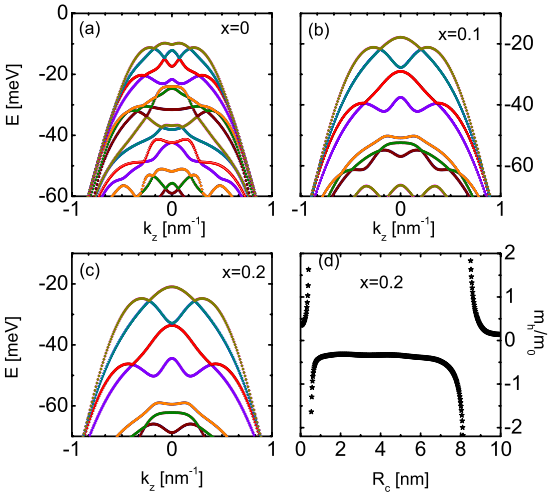

FIG. 5. (Color online) Valence band structure of $GaAs/Al_xGa_{1-x}As$ nanowires with $R_c=5$ nm and $R=10$ nm for (a) $x=0$, (b) $x=0.1$, (c) $x=0.2$ and the effective hole mass at $k_z=0$ (d) for $x=0.2$ and $R_c=1-10$ nm and $R=10$ nm for a $GaAs/Al_xGa_{1-x}As$ nanowire in [001] growth direction.

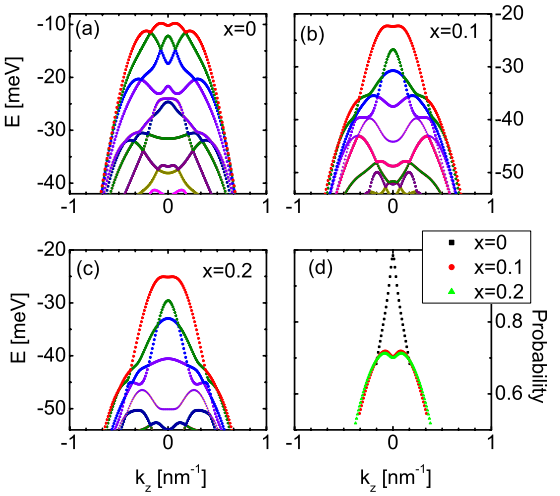

FIG. 6. (Color online) Valence band structure with (a) $x=0$, (b) $x=0.1$, (c) $x=0.2$, and light-hole spinor distributions for the top hole band (d) with $R_c=5$ nm and $R=10$ nm $Al_xGa_{1-x}As/GaAs$ nanowire in [001] growth direction.

split-off band can mix strongly with the heavy- and light-hole bands for thin wires. Therefore, all shown results are obtained with the 6×6 KL Hamiltonian. We have investigated wires with different radii but a representative example is the core-shell wire with a radius of $R=10$ nm.

Let us first consider a nanowire with a core of GaAs with radius $R_c=5$ nm, and an $Al_xGa_{1-x}As$ shell. Figure 5(a) shows the top of the valence band around $k_z=0$ for $x=0$, 0.1, and 0.2. For $x=0$ a clear camelback structure is found, as this is of course a pure GaAs nanowire. However, when the Al concentration in the shell is increased, we find the remarkable result that the camelback structure disappears, even for $x=0.1$. We summarized the R_c dependence of the camelback structure by calculating the effective mass at $k_z=0$ which we obtained by fitting $E=-\hbar^2k_z^2/2m_h$ around $k_z=0$. The results for $x=0.2$ and $R=10$ nm are plotted in Fig. 5(d). A negative mass corresponds to a camelback structure which is found in the ranges 0 nm$<R_c<$0.6 nm and 8 nm$<R_c<$10 nm. The transition point between positive and negative effective masses corresponds to a flat band around $k_z=0$ where $|m_h|=\infty$.

Similar results are shown in Figs. 6(a)–6(c) for nanowires with $Al_xGa_{1-x}As$ core and GaAs shell. The light-hole distribution is given in Fig. 6(d). Notice now that also in this case the camelback structure disappears with increasing Al concentration. Furthermore we observe a local minima in the light-hole distribution around $k_z=0$ for $x=0.1$ and $x=0.2$.

It is also interesting to look at the influence of the core radius on these results. Let us again consider a nanowire with a GaAs core. The Al concentration of the $Al_xGa_{1-x}As$ shell is fixed to $x=0.3$. Figure 7 shows the evolution of the top of the valence band for $R_c=0$, 2, 6, and 10 nm. Again we note that the camelback structure, which is present for $R_c=0$ nm and $R_c=10$ nm, immediately disappears in case of a core-shell structure. Also note that in Fig. 7(b) for $R_c=2$ nm the bands appear to be unevenly distributed in energy as compared to the other shown band structures. The reason is that for a $GaAs/Al_{0.3}Ga_{0.7}As$ nanowire the hole is more strongly confined within the core region for a core radius $R_c=2$ nm then for the other core radii, as will be shown in Sec. III D. Therefore, the spectrum resembles the spectrum of a thinner wire which has a smaller dispersion.

If we interchange the core and the shell materials, thus $Al_xGa_{1-x}As$ in the core and GaAs in the shell, the camelback structure also disappears, however not as abrupt as in the

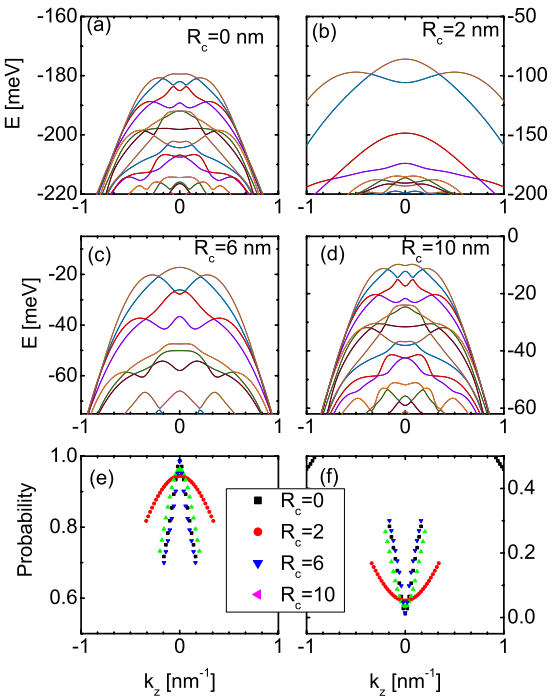

FIG. 7. (Color online) Valence band structure of $GaAs/Al_{0.3}Ga_{0.7}As$ nanowires with (a) $R_c=0$ nm, (b) $R_c=2$ nm, (c) $R_c=6$ nm, (d) $R_c=10$ nm and $R=10$ nm, and (e) light-hole and (f) heavy-hole distributions of the top valence band with $R=10$ nm.

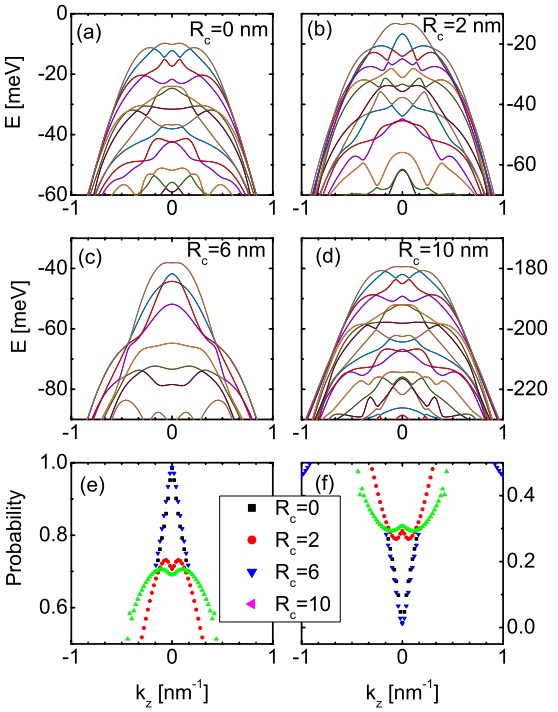

FIG. 8. (Color online) Valence band structure of $Al_{0.3}Ga_{0.7}As/GaAs$ nanowires with (a) $R_c=0$ nm, (b) $R_c=2$ nm, (c) $R_c=6$ nm, (d) $R_c=10$ nm, and (e) light-hole and (f) heavy-hole distributions of the top valence band with $R=10$ nm.

previous case, as shown in Fig. 8 for $x=0.3$. And again we see a maximum in the light-hole distribution and a minimum in the heavy-hole distribution when GaAs is in the core, and a minimum in the light-hole distribution and a maximum in the heavy-hole distribution when $Al_xGa_{1-x}As$ is in the core.

C. Optical absorption

Now that we have seen that the structure of the top of the valence band can change drastically in a core-shell nanowire in comparison to a single material wire, we will investigate its effect on the absorption spectrum. Again all shown results are for nanowires with a radius of $R=10$ nm.

The onset of the absorption peak is given by the energy difference $\Delta E=E_c-E_v$, where E_c is the lowest energy of the conduction band, E_v is the highest valence-band energy (note that E_g, the band gap of GaAs, is not included). This energy difference induced by quantum confinement is shown in Fig. 9(a) for GaAs in the core and in Fig. 9(b) for $Al_xGa_{1-x}As$ in the core for different Al concentrations, as function of the radius of the core R_c. As $Al_xGa_{1-x}As$ has a larger band gap than GaAs, this onset undergoes a blueshift when more Al is present in the wire.

It is now of interest to investigate the influence of the presence of a camelback structure on the absorption spectrum. Figures 10 and 11 show the evolution of the absorption spectra as function of the core radii, for nanowires with a radius of $R=10$ nm. Figure 10 shows the results for wires with a GaAs core while Fig. 11 shows the results for an $Al_xGa_{1-x}As$ core. The Al concentration is fixed to 0.4. Note

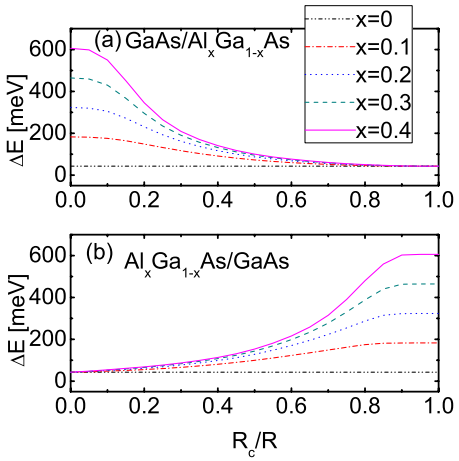

FIG. 9. (Color online) Quantum confinement induced energy shift $\Delta E=E_c-E_v$ in the electron (E_c) and hole (E_v) ground state for (a) $GaAs/Al_xGa_{1-x}As$ and (b) $Al_xGa_{1-x}As/GaAs$ nanowires with $R=10$ nm in [001] growth direction for different x values.

that peaks are present for lower energies near the onset of the absorption spectra in Figs. 10(a), 10(e), and 10(f) and Figs. 11(a) and 11(f). These are due to the camelback structure of the top valence band. The camelback structure causes the conduction band and the valence band to be equidistant around $k_z=0$, leading to a peak in the absorption spectrum. In case of Fig. 10(d) the large peak is due to the camelback structure in the second excited state [see Fig. 7(c)].

It is also interesting to look at the effect of the radius of the wire on these absorption spectra, as shown in Figs. 12–14. For thin wires the confinement effect is clearly visible as the different absorption peaks are clearly observable while in thicker wires the different peaks are not distinguishable

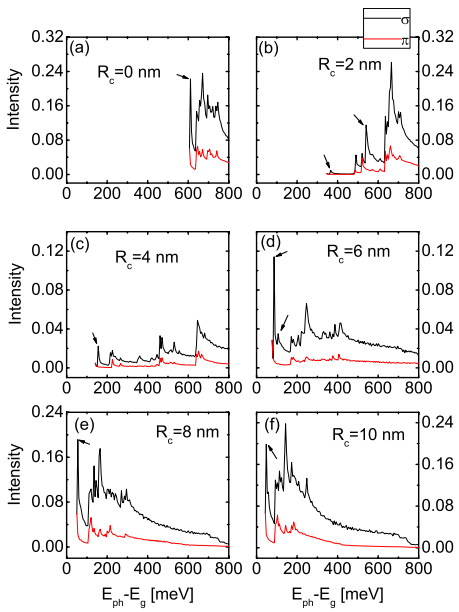

FIG. 10. (Color online) Absorption intensity (arbitrary units) for $GaAs/Al_{0.4}Ga_{0.6}As$ nanowire with (a) $R_c=0$ nm, (b) $R_c=2$ nm, (c) $R_c=4$ nm, (d) $R_c=6$ nm, (e) $R_c=8$ nm, and (f) $R_c=10$ nm and $R=10$ nm in [001] growth direction with 6×6 KL.

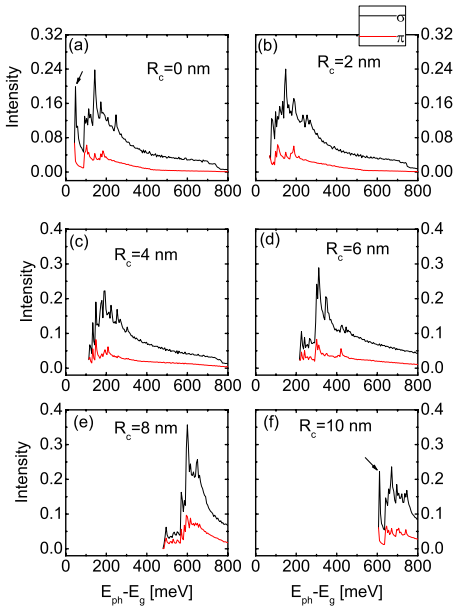

FIG. 11. (Color online) Absorption intensity (arbitrary units) for $Al_{0.4}Ga_{0.6}As/GaAs$ nanowire with (a) $R_c=0$ nm, (b) $R_c=2$ nm, (c) $R_c=4$ nm, (d) $R_c=6$ nm, (e) $R_c=8$ nm, and (f) $R_c=10$ nm and $R=10$ nm in [001] growth direction with 6×6 KL.

any more but they form a broad absorption band.

From the absorption results we can also see that there are certain energies for which the intensity peaks are only found for circularly polarized light (σ) and not for linearly polarized light (π). Examples are marked by arrows in Figs. 10 till 14. A look at Eqs. (14a) and (15) shows that these must be due to heavy hole→conduction-band transitions.

In Fig. 15 we give the degree of circular polarization (Π) for $GaAs/Al_xGa_{1-x}As$ nanowire for different x values for a particular case with $R_c=2$ nm [see Fig. 10(b)]. Here we see that as x changes from 0.1 to 0.4, the degree of circular polarization (Π) changes from positive to negative values (identified by arrows in Fig. 15). This shows that for these values initially, $I_{\sigma_+} \gg I_{\sigma_-}$ and then $I_{\sigma_+} \ll I_{\sigma_-}$. And from Eqs. (14a) and (15) we may conclude that for positive Π values

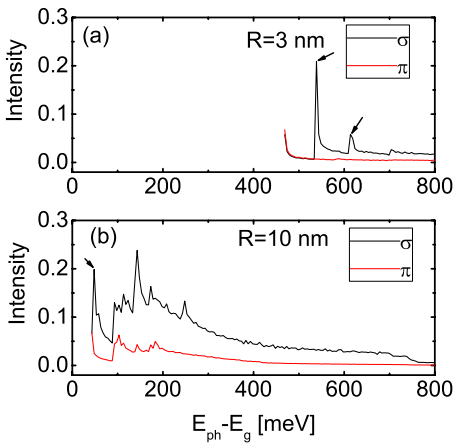

FIG. 12. (Color online) Absorption intensity (arbitrary units) for freestanding GaAs nanowire of radius (a) $R=3$ nm and (b) $R=10$ nm in [001] growth direction with 6×6 KL.

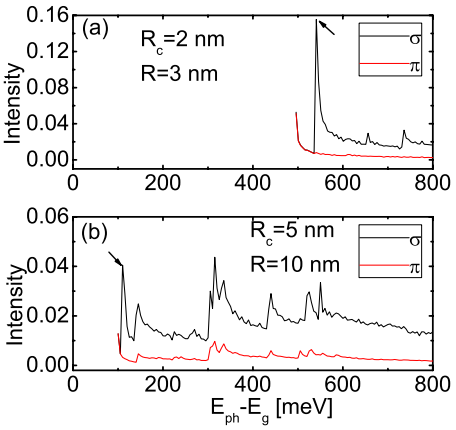

FIG. 13. (Color online) Absorption intensity (arbitrary units) for $GaAs/Al_{0.4}Ga_{0.6}As$ nanowire of (a) $R_c=2$ nm and $R=3$ nm and (b) $R_c=5$ nm and $R=10$ nm in [001] growth direction with 6×6 KL.

electrons with spin ↓ and for negative Π values electrons with spin ↑ are preferentially excited in the conduction band. Thus depending on whether left- or right-handed circularly polarized light is used, at certain energies, spin-polarized electrons can be obtained. For example, the positive peak in Fig. 15(d) (identified by an arrow) shows that left-handed circularly polarized light (σ_+) of energy $E=520.67$ meV can excite spin-↓ electrons with higher probability.

An interesting aspect of the camelback structure of the top of the valence band is its effect on the lifetime of the exciton: a k-indirect transition would occur with a strongly reduced transition probability giving rise to long recombination times. This suggests that the lifetime of the exciton is larger in pure wires where a camelback structure exists in comparison with core-shell nanowires where there is a smaller or even no camelback structure. In fact, the opposite is the case, as will be shown in the next section where we investigate the radial localization of electron and hole in the nanowire.

D. Electron and hole probabilities

As an example we focus again on the nanowire with a radius of $R=10$ nm, and a core radius of $R_c=5$ nm. Figures 16(a) and 16(b) show the electron and hole densities, respec-

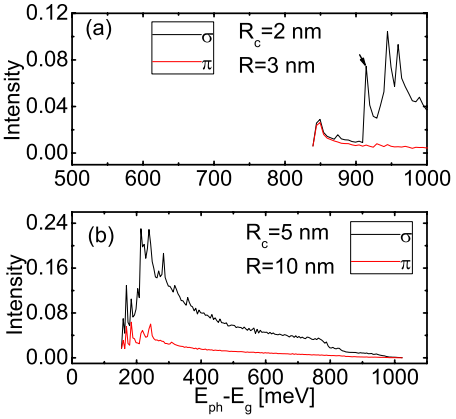

FIG. 14. (Color online) Absorption intensity (arbitrary units) for $Al_{0.4}Ga_{0.6}As/GaAs$ nanowire of (a) $R_c=2$ nm and $R=3$ nm and (b) $R_c=5$ nm and $R=10$ nm in [001] growth direction with 6×6 KL.

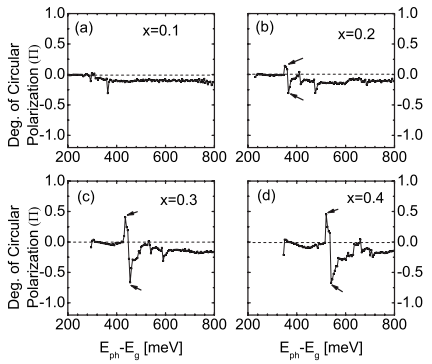

FIG. 15. Degree of circular polarization (Π) for GaAs/$Al_xGa_{1-x}As$ $R_c=2$ nm and $R=10$ nm with (a) $x=0.1$, (b) $x=0.2$, (c) $x=0.3$, and (d) $x=0.4$.

tively, at $k_z=0$ for a wire with a GaAs core, and Figs. 16(c) and 16(d) for a $Al_xGa_{1-x}As$ core, for different Al concentrations. For the wire with a GaAs core, increasing the Al concentration pushes the electron and hole more toward the center of the nanowire. The change in localization is however more pronounced in wires with an $Al_xGa_{1-x}As$ core. Even a small concentration of Al causes the hole to be pushed almost completely into the shell. Also the electron is pushed into the shell but still penetrates in the core due to its lighter mass in comparison to the holes. This change in localization due to the core-shell structure and the different impact on electrons and holes leads to a reduction in the overlap between electron and hole states. Figures 17(a)–17(d) show the average value of the radial position $\langle\rho\rangle(=\int\rho|\Psi|^2\rho d\rho)$ for wires with a GaAs and with a $Al_xGa_{1-x}As$ core, as function of the core radius R_c. From the average radial position of the electron and the hole it is apparent that the overlap of electron and hole wave functions is largely reduced in case of core-shell nanowires. Thus we predict that there will be a large increase in the exciton lifetime in core-shell nanowires as compared to single material nanowires.

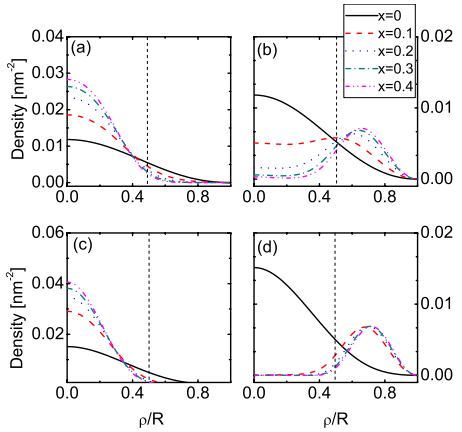

FIG. 16. (Color online) [(a) and (b)] Electron $[\Psi_{el}^2(\rho)]$ and [(c) and (d)] hole $[\Psi_h^2(\rho)]$ densities (of the ground state at $k_z=0$) for [(a) and (c)] GaAs/$Al_xGa_{1-x}As$ and [(b) and (d)] $Al_xGa_{1-x}As$/GaAs nanowires with $R_c=5$ nm and $R=10$ nm in [001] growth direction for different x values.

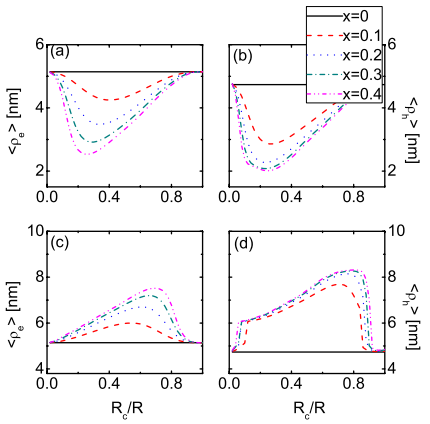

FIG. 17. (Color online) Average value of position $\langle\rho\rangle(\int\rho|\Psi|^2\rho d\rho)$ of [(a) and (c)] electrons and [(b) and (d)] holes (of the ground state at $k_z=0$) for [(a) and (b)] GaAs/$Al_xGa_{1-x}As$ and [(c) and (d)] $Al_xGa_{1-x}As$/GaAs nanowires with $R=10$ nm and $R_c=1-10$ nm in [001] growth direction for different x values.

IV. SUMMARY AND CONCLUSIONS

We have investigated the electronic structure of GaAs/$Al_xGa_{1-x}As$ and $Al_xGa_{1-x}As$/GaAs core-shell nanowires grown in the [001] direction using the 6×6 Kohn-Lüttinger $\mathbf{k}\cdot\mathbf{p}$ Hamiltonian. We showed that the 4×4 model breaks down for thin nanowires. It is also shown that the camelback structure of the top of the valence band around $k_z=0$, which is present in pure GaAs nanowires, slowly disappears with increasing Al concentration. We found that the camelback structure is not always present in core-shell structures. When GaAs is the core material, the evolution of the camelback structure as function of the core radius is almost independent of the Al concentration, while for wires with a GaAs shell, the region in which a camelback structure can be observed is larger for smaller Al concentration.

We also calculated the absorption spectra for different polarized light and found that a change in the effective mass of electrons and holes in the ground state is reflected in the absorption spectra: a camelback structure leads to a peak in the absorption spectrum because the top of the valence band and the bottom of the conduction band are equally aligned in some part of the Brillouin zone. We find a broad absorption spectra for thick wires but for thin wires many more absorption peaks are observable due to the quantum confinement effect. We predict that spin-polarized electrons can be obtained by using circularly polarized light for specific energies.

Wires with a GaAs core localize both the electron and the hole in the core region while wires with a $Al_xGa_{1-x}As$ core push them to the shell region. In both cases the core-shell structure leads to a spatial separation of the electron and the hole, which will lead to an increase in the lifetime of the exciton.

ACKNOWLEDGMENTS

This work was supported by the Flemish Science Foundation (FWO-Vl) and the Belgian Science Policy (IAP).

[1] R. S. Wagner and W. C. Ellis, Appl. Phys. Lett. **4**, 89 (1964).
[2] Z. H. Wu, X. Y. Mei, D. Kim, M. Blumin, and H. E. Ruda, Appl. Phys. Lett. **81**, 5177 (2002).
[3] J. Westwater, D. P. Gosain, S. Tomiya, S. Usui, and H. Ruda, J. Vac. Sci. Technol. B **15**, 554 (1997).
[4] J. Hu, M. Ouyang, P. Yang, and C. M. Lieber, Nature (London) **399**, 48 (1999).
[5] A. M. Morales and C. M. Lieber, Science **279**, 208 (1998).
[6] H. Y. Li, O. Wunnicke, M. T. Borgstrom, W. G. G. Immink, M. H. M. van Weert, M. A. Verheijen, and E. P. A. M. Bakkers, Nano Lett. **7**, 1144 (2007).
[7] K. Haraguchi, T. Katsuyama, K. Hiruma, and K. Ogawa, Appl. Phys. Lett. **60**, 745 (1992).
[8] X. Duan, J. Wang, and C. M. Lieber, Appl. Phys. Lett. **76**, 1116 (2000).
[9] A. Shabaev and A. L. Efros, Nano Lett. **4**, 1821 (2004).
[10] M. H. Huang, S. Mao, H. Feick, H. Yan, Y. Wu, H. Kind, E. Weber, R. Russo, and P. Yang, Science **292**, 1897 (2001).
[11] Y. Shiratori and S. Kasai, Jpn. J. Appl. Phys. **47**, 3086 (2008).
[12] A. Mikkelsen, N. Skőld, L. Ouattara, M. Borgstorm, J. N. Andersen, L. Samuelson, W. Seifert, and E. Lundgren, Nature Mater. **3**, 519 (2004).
[13] M. Tchernycheva, C. Sartel, G. Cirlin, L. Travers, G. Patriarche, J. C. Harmand, L. S. Dang, J. Renard, B. Gayral, L. Nevou, and F. Julien, Nanotechnology **18**, 385306 (2007).
[14] L. J. Lauhon, M. S. Gudiksen, D. Wang, and C. M. Lieber, Nature (London) **420**, 57 (2002).
[15] T. B. Hoang, L. V. Titova, J. M. Yarrison-Rice, H. E. Jackson, A. O. Govorov, Y. Kim, H. J. Joyce, H. H. Tan, C. Jagadish, and L. M. Smith, Nano Lett. **7**, 588 (2007).
[16] J. A. Czaban, D. A. Thompson, and R. R. LaPierre, Nano Lett. **9**, 148 (2009).
[17] E. D. Minot, F. Kelkensberg, M. van Kouwen, J. A. van Dam, L. P. Kouwenhoven, V. Zwiller, M. T. Borgstrm, O. Wunnicke, M. A. Verheijen, and E. P. A. M. Bakker, Nano Lett. **7**, 367 (2007).
[18] B. Hua, J. Motohisa, Y. Kobayashi, S. Hara, and T. Fukui, Nano Lett. **9**, 112 (2009).
[19] J. Wang, M. S. Gudiksen, X. Duan, Y. Cui, and C. M. Lieber, Science **293**, 1455 (2001).
[20] Y. Cui, Z. Zhong, D. Wang, W. U. Wang, and C. M. Lieber, Nano Lett. **3**, 149 (2003).
[21] G. Fishman, Phys. Rev. B **52**, 11132 (1995).
[22] J. B. Xia, Phys. Rev. B **43**, 9856 (1991).
[23] M. E. Pistol and C. E. Pryor, Phys. Rev. B **78**, 115319 (2008).
[24] G. E. Pikus and G. L. Bir, Fiz. Tverd. Tela (Leningrad) **1**, 1642 (1959) [Sov. Phys. Solid State **1**, 1502 (1960)].
[25] G. L. Bir and G. E. Pikus, *Symmetry and Strain-Induced Effects in Semiconductors* (Wiley, New York, 1974).
[26] W.-H. Seo and J. F. Donegan, Phys. Rev. B **68**, 075318 (2003).
[27] J. M. Luttinger and W. Kohn, Phys. Rev. **97**, 869 (1955).
[28] T. Dietl, H. Ohno, and F. Matsukura, Phys. Rev. B **63**, 195205 (2001).
[29] A. Baldereschi and N. O. Lipari, Phys. Rev. B **8**, 2697 (1973).
[30] I. Vurgaftman, J. R. Meyer, and L. R. Ram Mohan, J. Appl. Phys. **89**, 5815 (2001).
[31] W. Yi, V. Narayanamurti, H. Lu, M. A. Scarpulla, A. C. Gossard, Y. Huang, J.-H. Ryou, and R. D. Dupuis, Appl. Phys. Lett. **95**, 112102 (2009).
[32] P. Y. Yu and M. Cardona, *Fundamentals of Semiconductors*, 3rd ed. (Springer, New York, 2003), p. 260.
[33] P. Redliński and F. M. Peeters, Phys. Rev. B **77**, 075329 (2008).